Nonexponential distributions of tail states in hydrogenated amorphous silicon

Monica Brinza,* Evguenia V. Emelianova, and Guy J. Adriaenssens
Laboratorium voor Halfgeleiderfysica, University of Leuven, Celestijnenlaan 200D, B-3001 Leuven, Belgium
(Received 14 August 2004; revised manuscript received 26 October 2004; published 28 March 2005)

The analysis of the time-of-flight (TOF) photocurrent transients that leads to the identification of exponential band tails in hydrogenated amorphous silicon (*a*-Si:H), also predicts an electric-field dependence of the carrier drift mobilities. To account for *a*-Si:H samples, prepared in different ways and deposition rates, that do not show this field dependence of the drift mobility, general analytic expressions for the trap-limited-band-transport TOF signals were examined with nonexponential tail-state distributions. It is found that the use of a Gaussian tail-state component makes it possible to match the experimental curves when a field-independent mobility is measured. For samples that are prepared at, or close to, the conditions used for the plasma-enhanced chemical vapor deposition of standard "device-quality" *a*-Si:H, a purely exponential distribution does afford a good description of the experimental data. However, for samples prepared at high deposition rates in an expanding thermal plasma, or for polymorphous silicon, a significant Gaussian component is resolved in the tail-state distribution. These components can be linked to the presence in the amorphous matrix of nanoscopic more ordered silicon regions.

DOI: 10.1103/PhysRevB.71.115209 PACS number(s): 71.23.Cq, 72.80.Ng, 73.50.Pz, 61.43.Dq

I. INTRODUCTION

While an exponential distribution of tail states has been widely accepted[1] as offering a good description of the density of localized states near the mobility edge of both valence and conduction bands in hydrogenated amorphous silicon (*a*-Si:H), discrepancies between experimental data and the theoretical model have always been observed. But given the fact that comparisons are generally based on approximate solutions of the multiple-trapping (MT) transport model, those discrepancies were mostly thought to be related to the simplified approach and hence not further investigated. However, the use of such simplifications is not inevitable since detailed formulations of MT transport are available. In this paper we will employ the analytical MT expressions developed by Rudenko and Arkhipov[2] to examine *a*-Si:H tail-state distributions.

The main experimental evidence for exponential tail-state distributions has been derived from time-of-flight (TOF) transient photoconductivity measurements.[1] The current transients that are observed in that experiment show power-law behavior, $I_{\mathrm{ph}} \propto t^{-\beta}$, with different values for β before and after the time t_T that marks the transit of a carrier packet generated at $t=0$. MT theory predicts that for an exponential density of states (DOS), $g(E) \propto \exp(-E/E_0)$, where E is the energy of a localized state and E_0 represents the width of the distribution, the parameter β will take the values $1-\alpha$ and $1+\alpha$ for pre- and post-transit slopes, with $\alpha = kT/E_0$, k being the Boltzmann constant and T the temperature. However, actual experimental values mostly reveal $1-\alpha_1$ and $1+\alpha_2$, with $\alpha_1 \neq \alpha_2$. It was shown by Marshall *et al.*[3] how other than exponential distributions would be able to account for the measured slopes, but no attempt was made to fit experimental data. Yet, as is demonstrated by the present study, by extracting a more detailed image of the tail-state distribution than just the best exponential approximation to it and by focusing on more than just the current slopes, valuable detailed information can be obtained about the structure of particular *a*-Si:H samples. Specifically, evidence for nanoscale structure in polymorphous Si and in high-deposition-rate material prepared in an expanding thermal plasma (ETP) can be deduced from the field independence of the drift mobility, but a more general index of material homogeneity may be available.

While Marshall *et al.* used Monte Carlo simulation techniques to generate the transient current traces, the analytical expressions that are available in Refs. 2 and 4 offer a comprehensive alternative for studying the influence of different tail-state distributions on the transport parameters and to compare them systematically with experimental TOF data. Below, we will first discuss those aspects of TOF spectroscopy that do play a role in the analysis of the DOS in *a*-Si:H band tails. Next, the essentials of the analytical multiple-trapping transport model will be recapitulated with respect to their application in the modeling of experimental TOF current transients. Finally, we will present our analysis of the density of tail states in a number of *a*-Si:H samples that have been prepared in different ways, and that show remarkably different characteristics.

II. TIME-OF-FLIGHT TRANSIENT PHOTOCONDUCTIVITY

For time-of-flight transient photoconductivity experiments on *a*-Si:H, the layer to be examined is sandwiched between metallic contacts that form Schottky barriers at the interface, or between doped *a*-Si:H layers in a *p-i-n* geometry. At least one of the contacts is made semitransparent to allow free-carrier generation in the sample by means of a short pulse of strongly absorbed light. Shortly before the light pulse is triggered, an electric field is applied across the sample such that—depending on the polarity of the field or the orientation of the *p-i-n* cell—photogenerated electrons or holes will drift through the sample. A primary photocurrent will be mea-

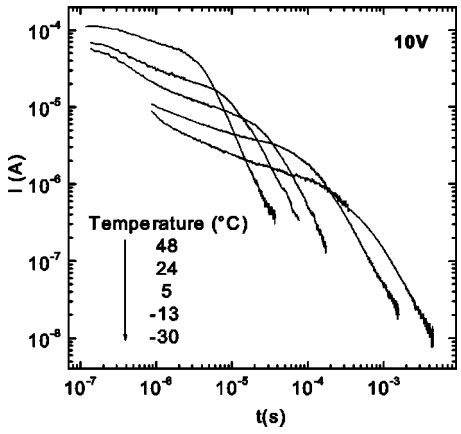

FIG. 1. Example of TOF hole transients measured at several temperatures as indicated, with 10 V applied across a 5.6-μm-thick ETP sample grown at 0.85 nm/s deposition rate, 250 °C substrate temperature, and sandwiched between Mo contacts.

sured in an external circuit due to the charge displacement in the sample, but secondary photocurrents will be blocked by the potential barriers at the interfaces.

Except well below room temperature, carrier motion in *a*-Si:H will take place at the mobility edge, but with carriers being repeatedly trapped in and released from the localized states in the *a*-Si:H band gap. (A brief outline of the relevant elements of this MT transport mode will be given in the next section.) While carrier trapping invariably occurs on a time scale that may be considered immediate on the scale of the TOF experiment ($\sim 10^{-12}$ s vs 10^{-8} s and longer), carrier release depends on the depth of individual traps since it is governed by a probability proportional to $\exp(-E_t/kT)$, with E_t being the trap depth. Consequently, since the localized states are distributed in energy, the photogenerated carrier packet will spread out during its transit through the sample, making the defining of a transit time for the packet a matter of convention. But, as shown by Seynhaeve *et al.*,[5] all conventional definitions correspond more or less to the time defined by the theoretical concept of the time it would take the mean of the carrier distribution to travel the length L of the actual sample in a semi-infinite medium. This definition will be used in the next section.

Charge trapping will also contribute to a nonequilibrium transport regime and decreasing currents of the type shown in Fig. 1. Those transient currents can be approximated by different power laws on either side of the transit time:

$$I_{\mathrm{ph}}(t) \propto \begin{cases} t^{-(1-\alpha_1)}, & t < t_T, \\ t^{-(1+\alpha_2)}, & t > t_T, \end{cases} \tag{1}$$

and the intersection of those power laws is often used as an experimental definition of t_T. It is the definition that was used in the present study. Current shapes of the type shown in Fig. 1 testify to the anomalously dispersive nature of the carrier transport. In the equilibrium transport regime, the pretransit current will be constant in time, i.e., $\alpha_1=1$ will be found.

The measured TOF transit time t_T forms the basis for the calculation of the carrier drift mobility $\mu_d=L/t_TF$, where F represents the applied electric field. μ_d is the quantity that is mostly quoted when TOF results are reported. In order for μ_d to be a meaningful quantity, the field F should be constant across the sample and remain so during the carrier transit. These conditions require that the time between the application of the field and the observation of the carrier transit has to be small with respect to the dielectric relaxation time of *a*-Si:H (on the order of 1 ms), and that the photoinjected charge Q_0 be much less than CV, the charge maintained on the sample capacitance C by the applied voltage V. For *a*-Si:H, the $Q_0 \ll CV$ requirement results in a photogenerated carrier density that is much smaller than the total density of localized states N_t, which means that trap filling need not be taken into account in the description of the MT transport.

TOF studies of the *a*-Si:H tail-state distribution have made use of either the field and/or temperature dependence of the μ_d values, or the observed current slopes α_1, α_2. Most frequently, the experimental data were examined only in terms of the expected exponential distribution of states, $g(E)=g(0)\exp(-E/E_0)$. Such distribution should result in a unique value for the slopes, $\alpha=\alpha_1=\alpha_2=kT/E_0$, and in a field dependence of the drift mobility according to

$$\mu_d \propto (L/F)^{1-1/\alpha}. \tag{2}$$

This analysis remains valid as long as $\alpha<1$, i.e., for temperatures less than E_0/k. In practice, the unique value of α is never obtained from the two slopes at more than one temperature,[6–8] and the direct proportionality between α and T is poorly obeyed.[8,9] Analysis of μ_d data sets as a function of temperature or applied field has led to other proposed distributions,[8,10–13] but they generally covered only a small part of the tail-state energy range or accounted for changes in just one of the experimental parameters. One intriguing result was obtained for the valence band tail of *a*-Si:H by Marshall *et al.*;[14] from an analysis of the field and temperature dependence of μ_d, they deduced a Gaussian tail-state distribution.

However, analysis of the TOF results need not be restricted to just the current slope or the drift mobility. Since good analytic descriptions of the TOF experiment are available,[2,4] they can be used to model the actual current transients in the time domain over the range of experimental fields and temperatures. It amounts to using the full information contained in the TOF transients rather than just part of it. As will become evident below from our application of this approach to experimental TOF photocurrents, details of the tail-state distribution in the region that lies too close to the transport path for direct time-resolved observation, can be probed through such modeling.

III. THEORETICAL MULTIPLE-TRAPPING TRANSPORT CONSIDERATIONS

Depending on the density of localized states and the temperature, electronic transport in disordered semiconductors will be dominated by either trap-limited band transport or hopping between localized states. Both processes have been extensively described in the literature in the past,[2,15] such that we may give here just a brief recapitulation of those specific aspects that will be called on in our analysis of the

TOF transients in *a*-Si:H. In fact, since our experimental data were all obtained at temperatures above 120 K where hopping becomes unimportant,[16] we just have to consider the trap-limited band transport, commonly referred to as multiple-trapping transport.

The MT transport model[2,17,18] predicts that, after excitation of the sample, an initial, nonequilibrium dispersive transport mode will occur that will terminate when the equilibrium distribution of localized carriers is established and equilibrium transport takes hold. The transition between the two regimes will occur sooner in a narrow or steeply decreasing DOS than in a broadly distributed one, and will in fact never take place in an unlimited exponential distribution.

A description of charge carrier transport in amorphous materials will be based on the continuity equation and an equation that relates the carrier density to the ongoing carrier trapping and release processes:

$$e\partial n(x,t)/\partial t + \partial j_c(x,t)/\partial x = 0, \tag{3}$$

$$\partial\rho(x,t,E)/\partial t = (1/N_t\tau_0)g(E)n_0(x,t) - (N_c/\tau_0 N_t) \times \exp(-E/kT)\rho(x,t,E). \tag{4}$$

In the above equations, e is the elementary charge, x the spatial coordinate, t the time, j_c the conduction current density, n the total carrier density, n_0 the free-carrier density, $g(E)dE$ the density of localized states with energies between E and $E+dE$, and $\rho(E)dE$ the density of carriers in these states. N_t is the total density of localized states, N_c the effective density of states at the mobility edge (i.e., the transport path), and τ_0 the free-carrier lifetime. The total carrier density can be written as

$$n(x,t) = n_0(x,t) + \int_0^\infty dE\ \rho(x,t,E) \cong \int_0^\infty dE\ \rho(x,t,E), \tag{5}$$

where the approximate expression is appropriate for the experimentally accessible time domain of standard TOF experiments in amorphous semiconductors since the large majority of carriers will be trapped at any given moment. In the MT model only free carriers contribute to the current, such that the TOF current can be written as

$$j(t) = (e\mu_0 F/L)\int_0^L dx\ n_0(x,t), \tag{6}$$

where μ_0 is the free-carrier mobility.

The thin layer of free carriers that is photogenerated at the time $t=0$ at the front electrode in a TOF experiment corresponds to the following initial conditions:

$$n(x,0) = n_0(x,0) = \lambda\delta(x), \quad \rho(x,0,E) = 0, \tag{7}$$

where λ is the surface carrier density. Solving the above equations, it is possible to obtain general expressions for the carrier density and transient current.[2,4] However, those exact analytic expressions are complex and not convenient for comparison with experimental data. Fortunately, a relatively simple approximate solution of the problem can be obtained by making use of the demarcation energy concept whereby a time-dependent demarcation level $E_d(t)=kT\ln(\nu t)$ divides localized states into shallow and deep ones. The attempt-to-escape frequency ν corresponds to $N_c/\tau_0 N_t$. Carriers that are localized in shallow states with $0<E<E_d$ will be in thermal equilibrium with the free-carrier density n_0 as a result of the multiple trapping and release events they have undergone. The solution of Eq. (4) may then, for those carriers, be written as

$$\rho(x,t,E) = (\nu\tau_0)^{-1}[g(E)/N_t]\exp(E/kT)n_0(x,t), \quad 0 \leqslant E \leqslant E_d(t). \tag{8}$$

From the region of deep traps with $E>E_d(t)$, no carriers are released by the time t, such that only the trapping term of Eq. (4) needs be considered in that energy range:

$$\rho(x,t,E) = (1/\tau_0 N_t)g(E)\int_0^t dt' n_0(x,t'), \quad E > E_d(t). \tag{9}$$

After the initial photogeneration step of the TOF experiment, nonequilibrium conditions prevail with most carriers having been trapped below E_d. Under those circumstances and until the whole distribution has thermalized, an expression for the free-carrier density can be obtained by introducing the expression for $\rho(x,t,E)$ from Eq. (9) into Eq. (5):

$$n_0(x,t) = (\partial/\partial t)[\tau(t)n(x,t)], \tag{10}$$

where the function $\tau(t)$ is defined as

$$\tau(t) = \tau_0\left[(1/N_t)\int_{E_d(t)}^\infty g(E)dE\right]^{-1}, \tag{11}$$

and where use is made of the fact that $n_0 \ll n$. It will be noticed from Eq. (10) that the free-carrier density $n_0(x,t)$ depends *differentially* on the total carrier density n under the strongly nonequilibrium conditions of dispersive transport. The combination of Eqs. (5)–(10) makes it possible to calculate the shape of the TOF current transients for a known (or surmised) distribution of states $g(E)$ and specific values of the parameters N_t, τ_0, and μ_0. These calculated current transients can then be compared directly with experimental ones. The TOF transit time t_T is defined implicitly in the MT model by way of the expression for the spatial mean of the carrier packet

$$\langle x\rangle(t_T) = \int_0^\infty dx\ xn(x,t) \Big/ \int_0^\infty dx\ n(x,t)\Big|_{t=t_T} = \mu_0 F\tau(t_T) = L. \tag{12}$$

Since the function $\tau(t)$, and therefore also $\langle x\rangle(t)$, depend nonlinearly on time, the transit time t_T must be a nonlinear function of the ratio L/F and, therefore, the dispersive carrier drift mobility $\mu_d=(L/F)/t_T$ will depend upon the field and sample thickness. For an exponential DOS, $g(E) \propto \exp(-E/E_0)$, this functional dependence takes the form[4]

$$\mu_d = \mu_0\tau_0\nu\left[(L/F)/\mu_0\tau_0\right]^{1-1/\alpha}, \quad \alpha < 1, \tag{13}$$

i.e., the dependency that is frequently looked for in experimental data sets, as pointed out already in the previous section.

The use of the total density of localized states in the above expressions implies that the same energy-independent capture coefficient $(1/\tau_0 N_t)$ is assumed for all states. This assumption will be acceptable as long as trapping into tail states dominates the MT process, given that major differences in capture probability should only be expected between tail and gap states, the former being disorder induced while the latter relate to lattice defects and/or impurities. Since all TOF studies of *a*-Si:H to date concur that the transit time occurs with the demarcation energy still located in the band tail, the constant capture probability of the model is appropriate.

Different behavior will be observed in the TOF experiment when material properties are such that an equilibrium distribution of trapped carriers can be established within the experimental time frame. Such could be the case, for instance, with a Gaussian distribution of localized tail states. Experimental data should then be compared to expressions relying more on Eq. (8) for the thermalized carrier density rather than on Eq. (9). When carrier equilibration is completed, the entire operative part of the DOS distribution belongs to the zone of shallow traps. The relation between the total and free-carrier densities can then be written on the basis of Eq. (8) as

$$n_0 = n\nu\tau_0\left[\int_0^\infty dE[g(E)/N_t]\exp(E/kT)\right]^{-1} = \vartheta(T)n. \tag{14}$$

Equation (14) shows that in the equilibrium regime, n_0 and n are directly proportional to each other, unlike the nonequilibrium differential relationship found in Eq. (10). Substituting $n_0 = \vartheta(T)n$ in the equilibrium conduction current density $j_c = e\mu_0 F n_0$, and defining $\mu(T) = \mu_0\vartheta(T)$, one obtains

$$j_c = e\mu(T)Fn, \tag{15}$$

whereby the equilibrium trap-controlled mobility $\mu(T)$ is independent of time and the electric field F. The observation of a field- and thickness-independent TOF drift mobility is therefore generally taken as an important indication of equilibrium carrier transport.

As mentioned above, a Gaussian distribution of localized states offers favorable conditions for the observation of equilibrium transport within the time frame of a TOF experiment, but also a linearly decreasing DOS or any other distribution with a sufficiently steep decrease of the gap state density will allow equilibrium conditions to be realized. The presence of a dominant Gaussian DOS component of the type

$$g(E) = \frac{N_t}{\sigma\sqrt{2\pi}}\exp\left[\frac{-E^2}{2\sigma^2}\right], \tag{16}$$

where σ is the width of the distribution, can be recognized from the temperature dependence of the field-independent drift mobility $\mu(T)$. It will show a Gaussian temperature profile:

$$\mu(T) = \mu_0\nu\tau_0\exp[-\sigma^2/2k^2T^2]. \tag{17}$$

IV. EXPERIMENTAL RESULTS

Very striking examples of the possibilities of the analytical modeling are provided by the analysis of the TOF data obtained on *a*-Si:H samples prepared at high deposition rates by the expanding-thermal-plasma technique developed at the Eindhoven Technical University[19] and by polymorphous silicon samples from the École Polytechnique in Palaiseau.[20] In both cases, strong deviations from a presumed exponential DOS are required to account for the experimental data. While the presence of nanocrystalline Si particles in the polymorphous material is well documented,[21] similar inclusions are apparently to be found in the structure of ETP *a*-Si:H as well. Results from *a*-Si:H samples prepared by means of the standard plasma-enhanced chemical vapor deposition (PECVD) technique will be presented for comparison. In the latter case, a simple exponential tail does much better in accounting for the observed current traces.

A. TOF instrumentation

Experimental TOF data were obtained with the standard configuration consisting of a HP214B pulse generator for the applied field, a dye cell generating a 540 nm optical pulse of ~5 ns duration when triggered by a pulsed nitrogen laser (LSI 337), and an Iwatsu-8123 digital storage oscilloscope. Successive current transients with and without the laser being triggered are always measured and subsequently subtracted from each other to obtain the transient photocurrent. Measurement sequences are computer controlled. Samples were mounted in a vacuum chamber on a metal support, the temperature of which was regulated to better than 1 °C by a combination of liquid nitrogen cooling and electrical heating.

B. ETP samples

The ETP *a*-Si:H samples used in this study were prepared using SiH_4 and an expanding Ar-H_2 plasma.[19] Sandwich cells with either Cr or Mo Schottky barriers were deposited at Eindhoven University of Technology at rates of 6 to 7 nm/s, and substrate temperatures going from 250 to 450 °C. TOF samples with a *p-i-n* structure were grown at Delft University of Technology, at rates of 0.85 and 2 nm/s for substrate temperatures of 250 and 400 °C. The thickness of the intrinsic *a*-Si:H layer was several micrometers for all samples.

Figure 2(a) shows—in a double-logarithmic plot—hole drift mobility values as a function of the ratio L/F, from samples deposited at the lower deposition rate of 0.85 nm/s at 250 °C and measured at several temperatures. The exponent $(1-1/\alpha)$ of L/F seen in Eqs. (2) and (13) can be deduced from these data, and the value of α extracted at each temperature. Plotting those α values versus temperature, as in Fig. 2(b), a linear dependence of α on T emerges, but not the direct proportionality that would follow from an exponential tail-state distribution. From the slope of the dashed line in the figure a "best approximating" exponential with characteristic temperature $T_0 \cong 430$ K ($E_0 \cong 37$ meV) may

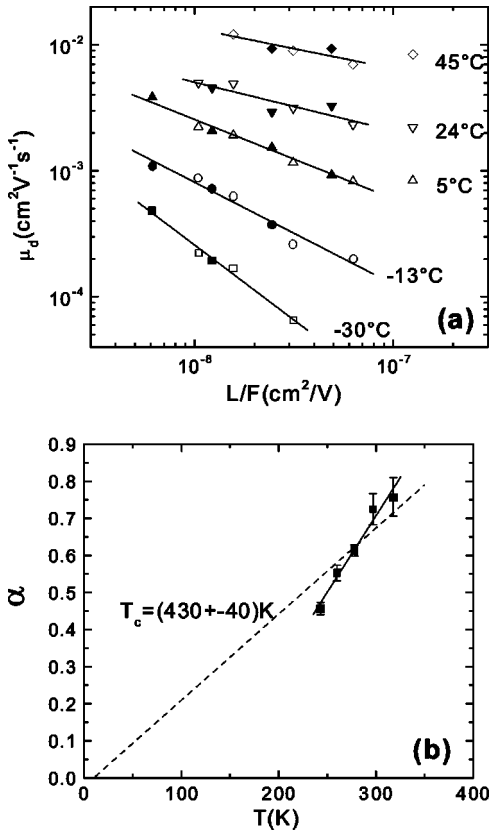

FIG. 2. (a) TOF hole drift mobility versus L/F ratio at the indicated measurement temperatures for samples deposited at 0.85 nm/s onto substrates held at 250 °C. Solid symbols refer to a 3.5-μm-thick *p-i-n* sample; open symbols relate to a 5.6-μm-thick sandwich cell with Mo Schottky barriers. (b) Values of the dispersion parameter α extracted from the data in (a) according to Eq. (13).

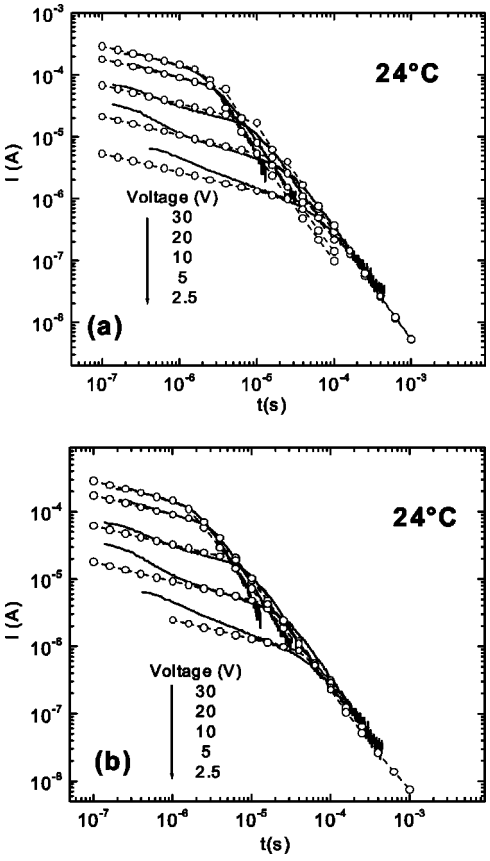

FIG. 3. Measured (full lines) and calculated (dashed lines +symbols) TOF current transients corresponding to 24 °C measurement temperature and applied voltages as indicated. The data are taken in the sample mentioned in Fig. 1. (a) The exponential DOS was used for calculations, with $N_{tE}=10^{21}$ cm^{-3}, $E_0=0.037$ eV, together with the values $\mu_0=6.8\times10^{-2}$ cm^2/V s, $\tau_0=10^{-11}$ s, and $N_c=10^{22}$ cm^{-3}. (b) The DOS of Eq. (18) was used for calculations, with $N_{tG}=5\times10^{20}$ cm^{-3}, $N_{tE}=10^{21}$ cm^{-3}, $E_0=0.04$ eV, $E_G=0.02$ eV, $\sigma=0.09$ eV, together with the values $\mu_0=0.65$ cm^2/V s, $\tau_0=10^{-11}$ s, and $N_c=1.3\times10^{21}$ cm^{-3}.

be deduced for the valence band tail. Although such approximations have been used in the past to support the notion of an exponential tail-state distribution, a direct comparison of TOF transients calculated on the basis of just a 430 K exponential and the actual experimental curves—as shown in Fig. 3—reveals the deficiencies of that approximation. In Fig. 3(a) the full lines show the experimental data while the dashed lines trace the results of the calculations. Modeling parameters were chosen to obtain close agreement with the highest-field curve, and then left unchanged for calculations at lower fields, except for small adjustments of the current amplitude that reflect similar small fluctuations of the laser intensity between individual measurements. It is clear from Fig. 3(a) that the field dependence of the actual transients varies from the one that would follow from a purely exponential tail. It is especially difficult to match pre- and post-transit slopes equally well, but for the sample at hand no significant errors in the determination of t_T would ensue. The agreement between experiment and calculation can be improved when a Gaussian component is added to the exponential one, and the values of the first parameter set are adjusted accordingly. The DOS then takes the form

$$g(E)=\frac{N_{tE}}{E_0}\exp\left(\frac{-E}{E_0}\right)+\frac{N_{tG}}{\sigma(2\pi)^{1/2}}\exp\left(\frac{-(E-E_G)^2}{2\sigma^2}\right). \tag{18}$$

Calculations with this DOS and the parameter values listed in the figure caption are shown in Fig. 3(b). While the rms difference between measured and calculated $\log_{10}I$ values decreased from 4.5% to 3.5% for the 30 V curves and from 1.5% to 1.1% for the 5 V curves upon the addition of the Gaussian component, very similar values for the reduced χ^2 values indicate that these differences are not statistically significant. It need not surprise, of course, that better agreement can be obtained with more fitting parameters, but it does demonstrate that the band tail is more structured than a single exponential can describe. Nevertheless, the fitting parameters show that the exponential function is the dominant one for the ETP deposition at moderate rate 0.85 nm/s and 250 °C. When comparing measured and calculated curves, it should be taken into consideration that discrepancies at the

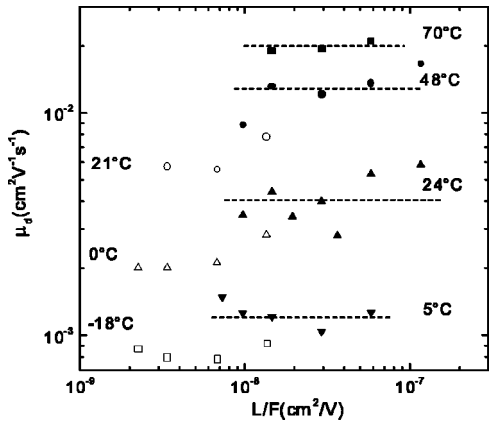

FIG. 4. Hole drift mobility, measured at the indicated temperatures, as a function of L/F in an ETP sample deposited at 6.2 nm/s and 425 °C (open symbols) and in one deposited at 2 nm/s and 400 °C (closed symbols). Lines of constant mobility are given as guide to the eye.

short-time end of the traces are due to the *RC* time constant of the electronic circuit and—at the lower voltage—the contact potential at the barriers, neither of which is present in the simulations.

An entirely different behavior is observed for the field dependence of the drift mobility in samples deposited at substrate temperatures of 400 to 450 °C and deposition rates around 6 nm/s. These samples consistently show a hole drift mobility that exceeds the one routinely measured in standard PECVD material,[22,23] and the drift mobilities for either electrons or holes show little or no dependence on the applied electric field. Hole drift mobility values from two samples are shown in Fig. 4 to illustrate this insensitivity to the field. As pointed out above, a field-independent drift mobility is generally associated with equilibrium transport, but the constant pretransit current that is expected in that case fails to be observed for these ETP samples. Indeed, as shown by the current traces displayed in Fig. 5, the general behavior of the transients is decidedly dispersive. An exponential distribution of tail states cannot reconcile these two characteristics.

Consequently, in an effort to match the field-independent drift mobility with the dispersive character of the transient signals of the ETP material, the analytical expressions for the TOF transients were used to calculate currents generated by multiple trapping in a DOS with partly exponential and partly Gaussian character. For a sample similar to the ones used for Fig. 4 (sample RS604 from Ref. 22, deposited at 5.6 nm/s and 450 °C), good agreement between measured and calculated curves was obtained with the DOS of Eq. (18) and the parameters $N_{tE}=6\times10^{18}$ cm^{-3}, $E_0=0.04$ eV, $N_{tG}=5\times10^{19}$ cm^{-3}, $\sigma=0.087$ eV, and $E_G=0.06$ eV. In contrast to the previous example (Fig. 3), it is now the Gaussian component that dominates the DOS in that part of the band tail that determines the TOF transit time. Examples of the calculated current traces have been added (dashed lines and symbols) to the actually measured ones (full lines) in Fig. 5. It remains possible to get a comparable fit to an individual experimental trace with just an exponential tail (the 6.4 V, −38 °C trace of Fig. 5 was used), but then the deviations

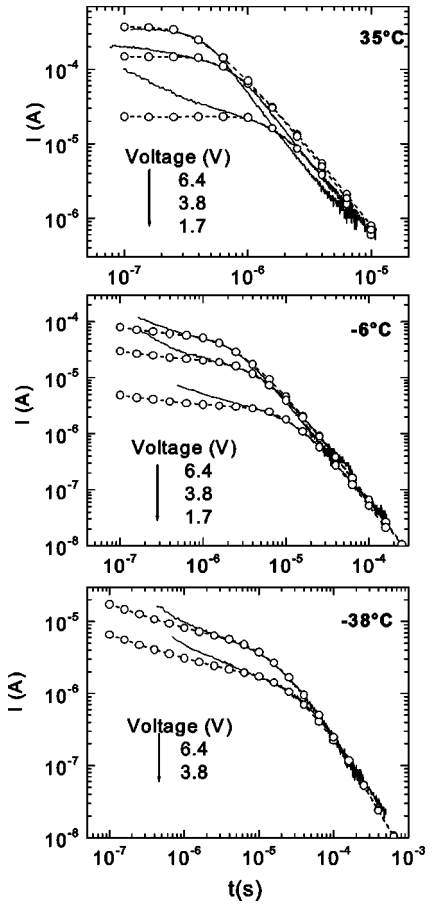

FIG. 5. Measured (full lines) and calculated (dashed lines +symbols) TOF current transients at indicated temperatures and applied voltages from a 2.4-μm-thick ETP *a*-Si:H sample, deposited at 450 °C and 5.6 nm/s, and measured with Cr Schottky barriers. The DOS of Eq. (18) was used for the calculations, with $N_{tG}=5\times10^{19}$ cm^{-3}, $N_{tE}=6\times10^{18}$ cm^{-3}, $E_0=0.04$ eV, $E_G=0.06$ eV, $\sigma=0.087$ eV, $\mu_0=0.10$ cm^2/V s, $\tau_0=10^{-11}$ s, and $N_c=2\times10^{21}$ cm^{-3}.

between calculation and experiment become unacceptably large at other fields and temperatures. (An example appears in the next section.) Consequently, for judging the appropriateness of the utilized DOS, it is necessary to examine both the field dependence and the temperature dependence of the calculated curves, as is done in the case of Fig. 5. Discrepancies at the short-time end of the traces are again due to the *RC* time constant of the electronic circuit at the shortest times and—at the lower voltage—the contact potential at the Schottky barrier, neither of which is taken into account in the simulations.

The transit times as well as the pre- and post-transit slopes measured with the high-deposition-rate samples are reproduced satisfactorily in the calculations, and the transit time is found to be independent of the applied field in the calculations just as it is in the experiment. Given that this field independence means that the Gaussian component of the DOS is dominant around the transit time, the temperature dependence of the mobility should agree with the Gaussian form of Eq. (17). That experimental drift mobility curves from ETP samples that were deposited at high substrate tem-

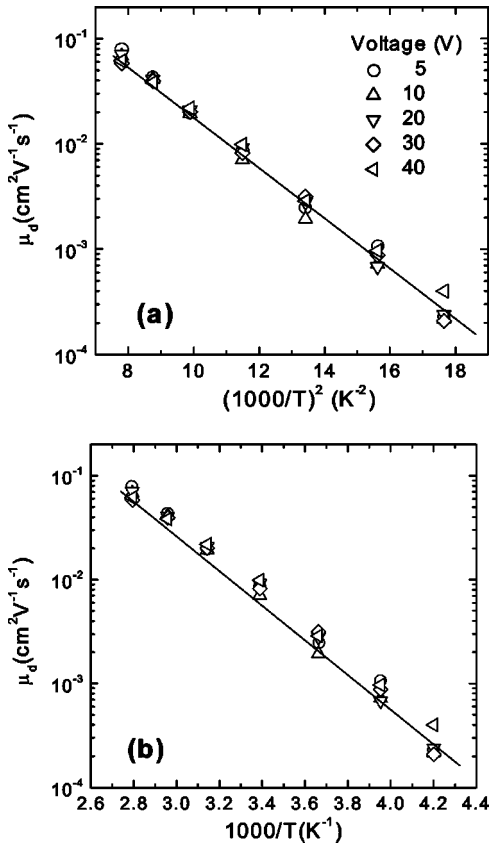

FIG. 6. Comparison of measured hole drift mobility plotted as $\log_{10}(\mu_d)$ versus $(1/T)^2$ and $(1/T)$. The essentially field-independent data were obtained with a 6.0-μm-thick ETP *a*-Si:H sample prepared at 6.1 nm/s and 425 °C, and with Cr contact layers. The lines are guides to the eye. Correlation coefficients for a straight-line fit to the data are $R=0.997\,04$ for (a) and $R=0.995\,66$ for (b).

peratures and/or high deposition rates do indeed fit an $\exp(T^{-2})$ law somewhat better than the traditional $\exp(T^{-1})$ is demonstrated for one such sample by Fig. 6. However, when taking into account that our comparison assumes that the parameters of Eq. (17) are not temperature dependent, the differences between Figs. 6(a) and 6(b) are too small to be significant.

Nevertheless, the combined evidence of experimental data and analytical calculations suggests that the DOS of ETP *a*-Si:H does contain both exponential and Gaussian components. While the Gaussian component dominates the TOF transients from material that is prepared at either high temperatures or high deposition rates, its presence can still be discerned in samples deposited at modest rates and lower substrate temperatures.

C. Polymorphous silicon

A series of polymorphous silicon *p-i-n* samples, deposited from a 2% SiH_4 and 98% H_2 mixture at varying total pressures from 133 to 232 Pa and 175 °C substrate temperature, was prepared at École Polytechnique, Palaiseau. The resulting TOF drift mobilities of electrons and holes have been

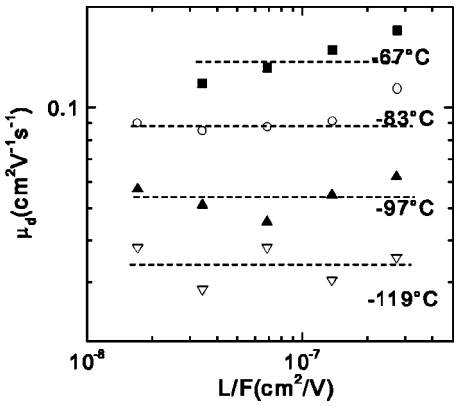

FIG. 7. Electron drift mobility plotted versus L/F for various temperatures as indicated. The measurements are performed in a 3.7-μm-thick polymorphous silicon sample deposited at 175 °C substrate temperature and 232 Pa total pressure in the reactor. Data are from Ref. 23; lines of constant mobility are given as guide to the eye.

reported in Ref. 24. Replotting the electron mobility data of the sample deposited under 232 Pa as a function of the applied field (Fig. 7), it is clear that the measured mobilities are essentially field independent. The equilibrium transport mode that is suggested by this result is also in accordance with the constant pretransit current levels that are seen for the experimental data (full lines) in Fig. 8. The dashed lines in Fig. 8 are theoretical calculations of the TOF transients on the basis of an exponential DOS with characteristic temperature $T_0=250$ K ($E_0=21.5$ meV), i.e., the most widely accepted conduction band tail value for *a*-Si:H,[1] and further parameters as shown in the figure caption. Those parameters, except for the actual sample length, were chosen to optimize the agreement between the calculated and measured curve at −97 °C with 8 V applied across the sample. The other curves were then calculated with the same parameter values, and only the temperature and applied voltage reset to the values used in the experiment. Neither the changes due to a variation of the applied field nor those due to temperature variations are reproduced to an acceptable degree. Using other values for T_0 did not lead to better results.

By again introducing a Gaussian component to the DOS, as in Eq. (18), much better agreement with the experimental data can be achieved. The results are shown in Fig. 9. As above, optimization of the parameters was carried out for the −97 °C, 8 V curve and the parameters were subsequently left unchanged for the other calculations. From the fitting parameters shown in the figure caption it can be seen that the amplitude of the Gaussian component, N_{tG}, is relatively more important here than the strength, N_{tE}, of the exponential part, in contrast to the ETP example of Fig. 3 where $N_{tE}>N_{tG}$ is required for reasonable agreement. For the ETP sample of Fig. 5 that does show field-independent drift mobility, the $N_{tG}>N_{tE}$ relationship is observed that is also found for polymorphous silicon.

D. PECVD *a*-Si:H

As a test for the fitting procedure, we also examined TOF transients obtained with an *a*-SiH *p-i-n* cell deposited at

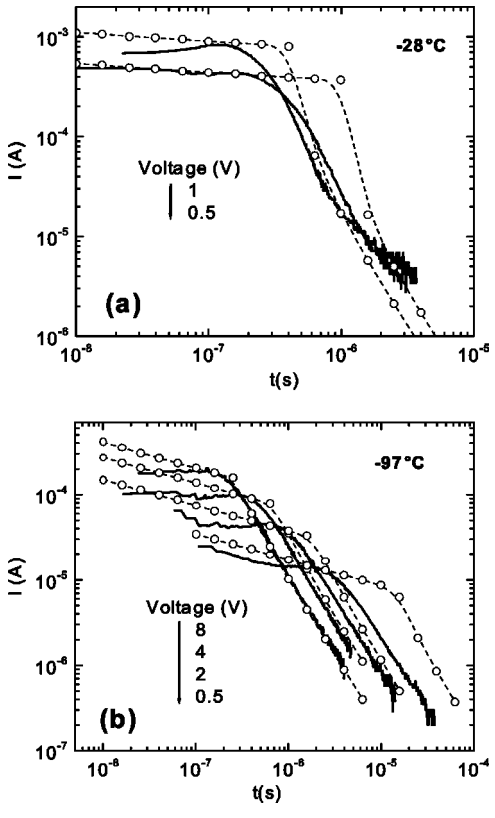

FIG. 8. Measured (full lines) and calculated (dashed lines +symbols) electron current transients in the sample referred to in Fig. 7 at two temperatures and various applied voltages as indicated. The exponential DOS was used for calculations, where $N_{tE}=10^{21}$ cm^{-3}, $E_0=0.022$ eV, together with the values $\mu_0=4$ cm^2/V s, $\tau_0=10^{-12}$ s, and $N_c=10^{21}$ cm^{-3}.

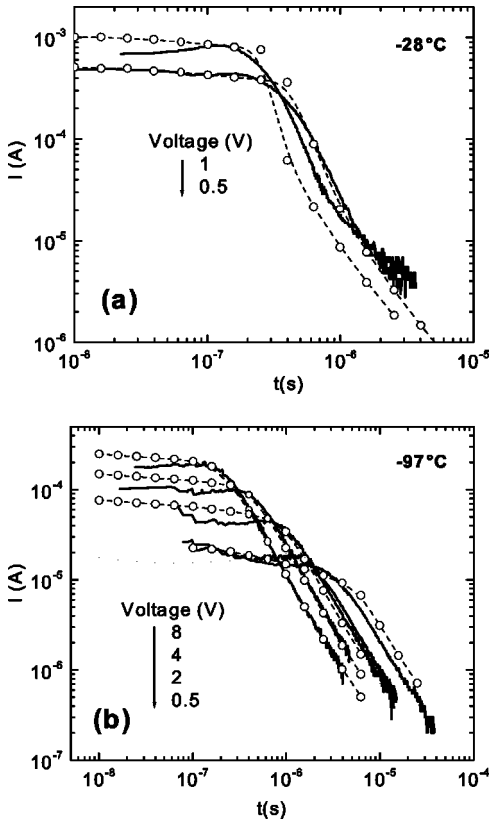

FIG. 9. Measured (full lines) and calculated (dashed lines+symbols) electron transients at temperatures −28 and −97 °C and applied voltages as indicated, for the sample mentioned in Fig. 7. The DOS of Eq. (18) was used for calculations, where $N_{tG}=5\times10^{20}$ cm^{-3}, $N_{tE}=2.5\times10^{20}$ cm^{-3}, $E_0=0.026$ eV, $E_G=0.06$ eV, $\sigma=0.04$ eV, together with the values $\mu_0=1.1$ cm^2/V s, $\tau_0=9\times10^{-12}$ s, and $N_c=7.2\times10^{21}$ cm^{-3}.

United Solar by means of standard plasma-enhanced chemical vapor deposition. Electron current transients measured at two temperatures and several applied voltages are displayed in Fig. 10, together with calculated traces on the basis of just an exponential tail with characteristic temperature $T_0=230$ K. The agreement between the two sets of curves is very good. In this case there is clearly not much to be gained from the introduction of a further DOS component. Or, expressed in a different way, for good-quality PECVD *a*-Si:H, an exponential tail-state distribution does fit the experimental data well, and there are no indications for any inhomogeneity that would require the addition of a Gaussian component to the tail.

V. DISCUSSION

It will have become clear from the preceding sections that a single-exponential distribution of tail states does not, in general, account for the various aspects of TOF transit signals in *a*-Si:H. For some samples, it even proves entirely unsatisfactory. It also has been demonstrated that the addition of a Gaussian component in the tail region of the DOS improves the agreement between experimental data and theoretical model. This last phenomenon does not just follow from the fact that more adjustable parameters become available through the Gaussian addition, but rather from the fundamentally different impact of exponential and Gaussian distributions on carrier transport in disordered systems.[25] In the latter distribution carriers can equilibrate while occupying states above the Fermi level, something that is not possible in an exponential tail. It is not surprising, therefore, that for samples like the high-deposition-rate ETP *a*-Si:H where the drift mobility exhibits equilibrium characteristics, an important Gaussian component is needed to describe the TOF transients. One aspect of the tail-state distribution that cannot be pinned down by the TOF modeling is the absolute density: The capture coefficient $(1/\tau_0 N_t)$ that is used in the calculations remains a free parameter in the model.

An important remaining question then concerns the physical origin of the Gaussian contribution to the density of tail states. It may be true that the physical origin of the accepted exponential tail-state distribution of "standard" *a*-Si:H is not exactly clear either, but that is beyond the scope of this discussion. Consequently we will accept that device-quality *a*-Si:H has tail-state distributions that are essentially exponentially distributed. As a corollary it may then be assumed that the exponential DOS component of Eq. (18) originates with a good-quality amorphous silicon background lattice in either the ETP *a*-Si:H or the polymorphous silicon, and that

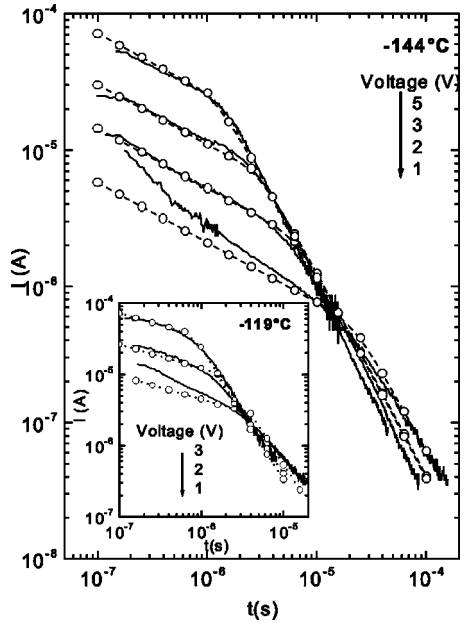

FIG. 10. Measured (full lines) and calculated (dashed lines +symbols) TOF current transients for electrons at temperatures −144 and −119 °C (inset) and applied voltages as indicated, in a 5.0-μm-thick PECVD sample. The exponential DOS was used for calculations, where $N_{tE}=10^{21}$ cm^{-3}, $E_0=0.02$ eV, together with the values $\mu_c=5.5$ cm^2/V s, $\tau_0=10^{-11}$ s, and $N_c=10^{21}$ cm^{-3}.

the Gaussian component finds its origin in random disturbances of the amorphous lattice. While it has been shown that the polymorphous material does indeed contain small paracrystalline inclusions,[21] we assume that the same holds for the ETP *a*-Si:H. In fact, a slight narrowing of the x-ray diffraction lines with increasing substrate temperature has been interpreted that way.[26] In addition, in the plasma that is used to grow the ETP *a*-Si:H layers, hydrogen-poor cationic silicon clusters were detected[27] that may play the same role as the incipient powder formation in the polymorphous silicon. The optical band gap of crystalline silicon is well below the 1.75 eV usually taken for *a*-Si:H, but quantum confinement in the small paracrystalline grains will result in a widening of that crystalline gap. In addition, the natural spread of grain sizes will result in a normal distribution of these enlarged crystalline gaps.

To assess the influence that such a distribution of gaps would have on the overall DOS in the gap of the ETP *a*-Si:H films, the band offsets between amorphous and crystalline phases have to be considered. Literature values for the valence band offset range from 0.4 to 0.6 eV,[28,29] and values in the neighborhood of 0.1 eV have been used for the conduction band offset.[30] Given that the band offset between amorphous and microcrystalline silicon is considerably larger at the valence band side than at the conduction band side, some gap widening due to the quantum confinement may roughly align the conduction band edges, but would still position the valence band edges of the crystalline inclusions inside the amorphous gap. Their normally distributed onsets can, therefore, be seen as the likely source of the Gaussian component in the tail-state distribution of the ETP *a*-Si:H valence band. It may be worth mentioning in this context that for recent

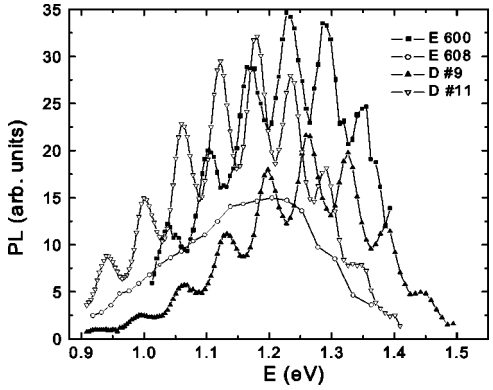

FIG. 11. Photoluminescence spectra of four ETP *a*-Si:H samples, two each from Eindhoven and Delft, spanning the range of examined deposition rates and temperatures, upon excitation with an Ar ion laser (2.41 eV).

modeling[31] of phototransport properties in hydrogenated microcrystalline silicon a Gaussian distribution of the valence band tail states was required to obtain acceptable results.

As an experimental probe for the presence of nanoscopic, structurally diverse inclusions in ETP *a*-Si:H, the photoluminescence spectra of several samples were studied. It is known that the presence of microcrystalline inclusions[32] or voids[33] in *a*-Si:H lowers the luminescence energy from the value near 1.4 eV that is normally observed for the homogeneous material to values in the 1.2 to 1.3 eV range. The luminescence spectra shown in Fig. 11 exhibit these lower radiative energies, thus suggesting the presence of similar inhomogeneities in the samples.

The presence in ETP *a*-Si:H of nanoscopic inclusions of the type discussed above could conceivably also play a role in the, so far, unpredictable nature of the electron drift mobility activation in the ETP TOF samples that were examined in this study. As pointed out already in an earlier report,[22] hole mobility values vary in a very regular way with sample preparation conditions, but the electron drift mobility shows erratic variations of its activation energy at lower temperatures that do not relate in any obvious way to sample preparation or prehistory. The differences do not persist above 250 K. As an example, Fig. 12 shows the low-temperature electron drift mobility measured in two samples deposited in equivalent circumstances. In one of the samples the electron drift mobility is more or less temperature activated as expected if transport takes place through multiple trapping in a distribution of tail states, while in the other the electron drift mobility is almost temperature independent, suggesting another transport mechanism. It was mentioned above that band offsets between amorphous and more ordered phases are expected to be minimal at the conduction band side of the gap. Small sample-to-sample variations could then result in either positive or negative band offsets, leading to significant changes in the transport mechanism for electronic conduction between individual samples. At the valence band side, where the band offset is larger, equally strong sample-to-sample variations would represent only relatively minor changes to the offset, and hence have only marginal influence on the hole conduction.

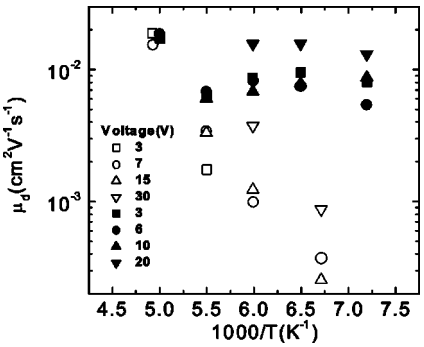

FIG. 12. Low-temperature behavior of the electron drift mobility measured at the indicated voltages in two *p-i-n* ETP samples, both of them grown at 0.85 nm/s deposition rate and 250 °C substrate temperature to a nominal thickness of 5.6 μm.

Following from the observation that, for all ETP samples studied, a purely exponential DOS is not able to account for the TOF results as well as the combination with a Gaussian component, it may be surmised that some nanostructure is present in those samples. Such structures would be in line with the recent model calculations by Nakhmanson *et al.*[34] for paracrystalline silicon whereby a few crystalline grains were embedded in a strain-distorted amorphous matrix in order to account for observed fluctuation electron microscopy signals of sputtered amorphous silicon.

VI. CONCLUSIONS

From comparisons between measured time-of-flight transient photocurrents and theoretical curves calculated on the basis of trap-limited band transport it emerges that an exponential density of states offers a good description for the band tails of device-quality PECVD *a*-Si:H. For material prepared at high deposition rates in an expanding thermal plasma, and for polymorphous silicon, an exponential DOS by itself fails to adequately describe the currents, but addition of a Gaussian component to the tail-state distribution remedies the problem. Evidence is given that the Gaussian component is linked to sample inhomogeneity, most likely the presence of nanoscopic more ordered silicon inclusions in the amorphous *a*-Si:H lattice. It follows that the relative importance of the exponential and Gaussian components in the tail-state distribution can be used as a measure of material homogeneity.

ACKNOWLEDGMENTS

The authors wish to thank Vladimir Arkhipov for his help with the finer points of the multiple-trapping transport model, Kostya Iakoubovskii for carrying out the photoluminescence measurements, and the Fonds voor Wetenschappelijk Onderzoek–Vlaanderen for financial support. We owe special thanks for sample preparation to Arno Smets (Eindhoven), Agnes Petit (Delft), Pere Roca i Cabarrocas (Palaiseau), and Baojie Yan (United Solar).

*Electronic address: monica.brinza@fys.kuleuven.ac.be

[1] R. A. Street, *Hydrogenated Amorphous Silicon* (Cambridge University Press, Cambridge, U.K., 1991).
[2] A. I. Rudenko and V. I. Arkhipov, Philos. Mag. B **45**, 177 (1982); **45**, 189 (1982); **45**, 209 (1982).
[3] J. M. Marshall, H. Michiel, and G. J. Adriaenssens, Philos. Mag. B **47**, 211 (1983).
[4] V. I. Arkhipov, M. S. Iovu, A. I. Rudenko, and S. D. Shutov, Phys. Status Solidi A **54**, 67 (1979).
[5] G. Seynhaeve, G. J. Adriaenssens, H. Michiel, and H. Overhof, Philos. Mag. B **58**, 421 (1988).
[6] T. Tiedje, J. M. Cebulka, D. L. Morel, and B. Abeles, Phys. Rev. Lett. **46**, 1425 (1981).
[7] P. B. Kirby, W. Paul, S. Ray, and J. Tauc, Solid State Commun. **42**, 533 (1982).
[8] J. M. Marshall, R. A. Street, and M. J. Thompson, Philos. Mag. B **54**, 51 (1986).
[9] T. Tiedje, in *Hydrogenated Amorphous Silicon II*, edited by J. D. Joannopoulos and G. Lucovsky (Springer-Verlag, Berlin, 1984), p. 261.
[10] M. Silver, E. Snow, and D. Adler, J. Appl. Phys. **59**, 3503 (1986).
[11] J. M. Marshall, J. Berkin, and C. Main, Philos. Mag. B **56**, 641 (1987).
[12] C. E. Nebel and G. H. Bauer, Philos. Mag. B **59**, 463 (1989).
[13] C. Longeaud, G. Fournet, and R. Vanderhaghen, Phys. Rev. B **38**, 7493 (1988).
[14] J. M. Marshall, R. A. Street, M. J. Thompson, and W. B. Jackson, Philos. Mag. B **57**, 387 (1988).
[15] A. Miller and E. Abrahams, Phys. Rev. **120**, 745 (1960); N. F. Mott, Philos. Mag. **19**, 835 (1969).
[16] D. Monroe, Phys. Rev. Lett. **54**, 146 (1985).
[17] F. W. Schmidlin, Phys. Rev. B **16**, 2362 (1977).
[18] J. Noolandi, Phys. Rev. B **16**, 4466 (1977).
[19] R. J. Severens, M. C. M. van de Sanden, H. J. M. Verhoeven, J. Bastiaanssen, and D. C. Schram, in *Amorphous Silicon Technology—1996*, edited by M. Hack, E. H. Schiff, S. Wagner, A. Matsuda, and R. Schropp, MRS Symposia Proceedings No. 420 (Materials Research Society, Pittsburgh, 1996), p. 341; W. M. M. Kessels, R. J. Severens, A. H. M. Smets, B. A. Korevaar, G. J. Adriaenssens, D. C. Schram, and M. C. M. Van de Sanden, J. Appl. Phys. **89**, 2404 (2001).
[20] P. Roca i Cabarrocas, P. Gay, and A. Hadjadj, J. Vac. Sci. Technol. A **14**, 655 (1996); P. Roca i Cabarrocas, J. Non-Cryst. Solids **266**, 31 (2000).
[21] G. Viera, M. Mikikian, E. Bertran, P. Roca i Cabarrocas, and L. Boufendi, J. Appl. Phys. **92**, 4684 (2002).
[22] M. Brinza, G. J. Adriaenssens, K. Iakoubovskii, A. Stesmans, W. M. M. Kessels, A. H. M. Smets, and M. C. M. van de Sanden, J. Non-Cryst. Solids **299**, 420 (2002). It should be noted that an unwarranted interpretation of the post-transit photocurrents in this paper was rectified in M. Brinza and G. J. Adriaenssens, J. Mater. Sci.: Mater. Electron. **14**, 749 (2003).
[23] S. Dinca, G. Ganguly, Z. Lu, E. A. Schiff, V. Vlabos, C. R.

Wronski, and Q. Yuan, in *Amorphous and Nanocrystalline Silicon-Based Films—2003*, edited by J. R. Abelson, G. Ganguly, H. Matsumura, J. Robertson, and E. A. Schiff, MRS Symposia Proceedings No. 762 (Materials Research Society, Pittsburgh, 2003), p. 345.

[24] M. Brinza, G. J. Adriaenssens, and P. Roca i Cabarrocas, Thin Solid Films **427**, 123 (2003).

[25] V. I. Arkhipov, P. Heremans, E. V. Emelianova, and G. J. Adriaenssens, Appl. Phys. Lett. **79**, 4154 (2001).

[26] A. H. M. Smets, Ph.D. thesis, Eindhoven University of Technology, 2002.

[27] W. M. M. Kessels, M. C. M. van de Sanden, and D. C. Schram, Appl. Phys. Lett. **72**, 2397 (1998).

[28] L. Ley, J. Reichardt, and R. L. Johnson, in *Proceedings of the 17th International Conference on the Physics of Semiconductors* (Springer, New York, 1984), p. 811.

[29] M. Sebastiani, L. Di Gaspare, G. Capellini, C. Bittencourt, and F. Evangelisti, Phys. Rev. Lett. **75**, 3352 (1995).

[30] J. M. Essick and J. D. Cohen, Appl. Phys. Lett. **55**, 1232 (1989); J. M. Essick, Z. Nobel, Y.-M. Li, and M. S. Bennett, Phys. Rev. B **54**, 4885 (1996).

[31] I. Balberg, Y. Dover, R. Naides, J. P. Conde, and V. Chu, Phys. Rev. B **69**, 035203 (2004).

[32] G. Yue, D. Han, D. L. Williamson, J. Yang, K. Lord, and S. Guha, Appl. Phys. Lett. **77**, 3185 (2000).

[33] D. Han, G. Yue, K. Wang, J. Baugh, Y. Wu, Y. Xu, and Q. Wang, Appl. Phys. Lett. **80**, 40 (2002).

[34] S. M. Nakhmanson, P. M. Voyles, N. Mousseau, G. T. Barkema, and D. A. Drabold, Phys. Rev. B **63**, 235207 (2001).